

Preparation of Ag/AgBr–Bi₂MoO₆ Plasmonic Photocatalyst Films with Highly Enhanced Photocatalytic Activity

Yujun Liu¹ · Feng Zhou¹ · Su Zhan¹ · Yifan Yang¹

Received: 7 March 2017 / Accepted: 22 May 2017 / Published online: 25 May 2017
© Springer Science+Business Media New York 2017

Abstract The novel plasmonic photocatalyst Ag/AgBr–Bi₂MoO₆ was successfully synthesized using a facile method. The composites were made into films in this study. The physical and photophysical properties of the as-prepared Ag/AgBr–Bi₂MoO₆ samples were characterized by X-ray diffraction, X-ray photo-electron spectroscopy, scanning electron microscopy, transmission electron microscopy, ultraviolet–visible diffuse reflection spectroscopy, photoluminescence emission spectroscopy, and electrochemical experiments. Photocatalytic activity was assessed through the decomposition of methylene blue in aqueous solution under visible light irradiation. The conclusion that Ag/AgBr species can improve the separation efficiency of charge carriers irradiated by visible light in Bi₂MoO₆ comes from the phenomenon that the higher photocatalytic property of all composites than that of pure Bi₂MoO₆. Moreover, 25 wt% Ag/AgBr–Bi₂MoO₆ exhibited 7.8 times higher degradation constant than that of the pure Bi₂MoO₆ and optimal photoactivity. The possible mechanism of the improvement of photocatalytic performance of Bi₂MoO₆ after introducing Ag/AgBr nanoparticles was discussed based on the theory of surface plasmon resonance effect from Ag species.

Keywords Ag/AgBr–Bi₂MoO₆ films · Visible-light · Photodegradation mechanism

1 Introduction

In the past few years, photocatalysis is widely used to solve environmental pollution and energy crisis because of its promising applications [1–4]. TiO₂ is a traditional photocatalyst with highly oxidized activity, stable performance, cost performance, and non-toxicity and is widely used in environmental purification [5–8]. However, TiO₂ could not make full use of solar energy because of its large band gap energy of about 3.2 eV.

Researchers specializing in photocatalysis have found several photocatalytic materials in the last few decades. In addition, Bi-based photocatalysts have been investigated intensively because of their particular crystalline structures, which are associated with the performance in the degradation of organic pollutants [9]. Bi₂MoO₆ with a small band gap (about 2.5–2.8 eV), which belongs to Bi-based photocatalysts, is one of the most promising catalysts because of its excellent visible light activities. In particular, Bi₂MoO₆ belongs to Aurivillius oxide family and consists of stacking of (Bi₂O₂)²⁺ layers and alternative perovskite (MoO₄)²⁺ slaps (Fig. 1) [10–13]. However, applications of Bi₂MoO₆ in the photocatalysis are greatly limited because of the high recombination efficiency of photogenerated electron–hole pairs [14, 15]. Thus, several studies have been carried out to overcome the limitations of Bi₂MoO₆. These methods are summarized as follows: (1) forming heterojunction, such as g-C₃N₄/Bi₂MoO₆ [16], TiO₂/Bi₂MoO₆ [17], P₃HT/Bi₂MoO₆ [18], and α-Fe₂O₃/Bi₂MoO₆ [19]; (2) ion doping: Gd³⁺ [20] and Ho³⁺ [21]; (3) changing morphology [22–24]; (4) self-doping [25]; and (5) surface sensitized [26]. Although the efforts have made much progress, the high recombination efficiency of photo-generated charge carriers restricts the application of Bi₂MoO₆.

✉ Feng Zhou
zhoufeng99@mails.tsinghua.edu.cn

¹ Key Laboratory of Ship-Machinery Maintenance and Manufacture for Ministry of Transport, Dalian Maritime University, Dalian 116026, China

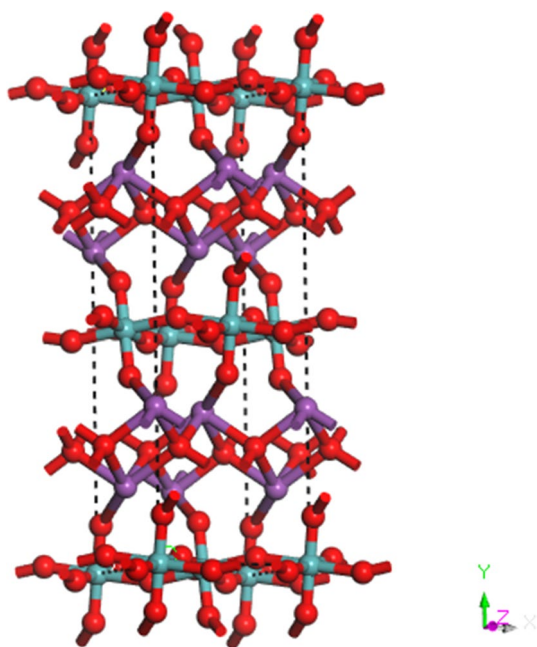


Fig. 1 Molecular structure of Bi_2MoO_6

Ag/AgX (Cl, Br, and I) have been used to perfect the semiconductor photocatalysts [27, 28]. The highly dispersed Ag/AgX species can enhance the photocatalytic activity of the substrates by improving the separation efficiency of electron–hole pairs. The improvement is attributed to Ag nanoparticles. Studies have proven that the Ag nanoparticles, which come in contact with a charged semiconductor, can effectively absorb visible light with surface plasmon resonance (SPR) effect. The electron product on the surface of Ag nanoparticles can transfer from metals to semiconductors after obtaining sufficient energy because of the SPR effect, which will participate in the photocatalytic reactions [29–36]. For example, Kato et al. have concluded that Ag^+ is significant to construct photocatalysts with narrow band gaps [37, 38]. Thus, to enhance the photocatalytic activity of Bi_2MoO_6 by introducing Ag/AgX species after the properties of Ag/AgX have been considered is practical and feasible.

In this work, highly active $\text{Ag}/\text{AgBr}-\text{Bi}_2\text{MoO}_6$ nanocomposites were fabricated by a facile approach successfully. The composite powders were made into films in a special method to improve utilization efficiency. The degradation of methylene blue (MB) is the most persuasive evidence to investigate the photocatalytic activity of $\text{Ag}/\text{AgBr}-\text{Bi}_2\text{MoO}_6$ films. The catalytic mechanism was explored based on experimental results and first principles. The outstanding property associated with $\text{Ag}/\text{AgBr}-\text{Bi}_2\text{MoO}_6$ composite material suggested that the introduction of Ag/AgBr with the SPR effect is beneficial to photocatalytic activity.

2 Experimental

2.1 Preparation of $\text{Ag}/\text{AgBr}-\text{Bi}_2\text{MoO}_6$ Composite Sample

2.1.1 Step 1: Preparation of Bi_2MoO_6

Solution A was prepared by adding 0.4 mol sodium molybdate (Na_2MoO_4) into 25 mL of nitric acid (1 mol/L). Briefly, 0.8 mol bismuth nitrate ($\text{Bi}(\text{NO}_3)_3$) was added into 25 mL of deionized water (labeled as solution B). Solutions A and B were mixed together with constant stirring, and the pH was adjusted to 1. The mixture solution was transferred into a Teflon-lined stainless steel autoclave after stirring for about 1 h. The autoclaves were heated at 180°C for 24 h. The produced solid materials were filtered and washed several times with deionized water and ethanol. The mixture was dried at 60°C for 6 h for further study.

2.1.2 Step 2: Synthesis of $\text{AgBr}-\text{Bi}_2\text{MoO}_6$

Approximately 1 g of the as-prepared Bi_2MoO_6 and 0.225 g of AgNO_3 powder were mixed in 20 mL of ethanol. The mixed solution (named solution C) was sonicated for about 1 h. Briefly, 0.1575 g of KBr (mass ratio of AgBr to Bi_2MoO_6 was 25%) was added to 20 mL of deionized water (named as solution D). The resulting suspension (mixture of solutions C and D) was stirred for 4 h at room temperature in the dark. The obtained samples were washed with deionized water.

2.1.3 Step 3: Obtaining $\text{Ag}/\text{AgBr}-\text{Bi}_2\text{MoO}_6$

Approximately 1 g of $\text{AgBr}-\text{Bi}_2\text{MoO}_6$ was dispersed into 20 mL of deionized water solution. Ag nanoparticles were obtained after the solution was exposed to a solar simulator (300 W Xe lamp) for 30 min. The samples were washed with ethanol and deionized water. The compounds were dried at 60°C for 12 h and named X wt% $\text{Ag}/\text{AgBr}-\text{Bi}_2\text{MoO}_6$ as BMO-X. Similarly, pure Ag/AgBr sample was prepared in the same manner.

2.2 Preparation of $\text{Ag}/\text{AgBr}-\text{Bi}_2\text{MoO}_6$ Film Electrodes

$\text{Ag}/\text{AgBr}-\text{Bi}_2\text{MoO}_6$ films were prepared on indium–tin oxide glass (ITO) using the drop coating method. First, 0.1 g of $\text{Ag}/\text{AgBr}-\text{Bi}_2\text{MoO}_6$ and 1 mg of XC-72 were dissolved in 1000 μL of methanol, 7000 μL of distilled water, and 3000 μL of polytetrafluoroethylene (PTFE) by ultrasonication for 10 min. Second, 600 μL of slurry was dipped onto ITO glass (20×20 mm) and then dried at 60°C for 2 h in the air. Only the carbon black XC-72 as conductive material can improve the electrical conductivity of the $\text{Ag}/$

AgBr–Bi₂MoO₆ film electrode. PTFE acts as film former agent.

2.3 Photocatalytic Experiment

The visible-light-driven photocatalytic activities of the Ag/AgBr–Bi₂MoO₆ films were evaluated by the degradation of MB. The light source is 300 W Xe lamp with a wavelength of light more than 420 nm. The average visible light intensity was 35 mW/cm⁻². In the typical procedure, the films were immersed into 50 mL MB solution (10⁻⁵ mol/L). The analytical samples of about 4 mL aliquots were taken every 15 min during the process of degradation experiment. The samples were examined on a UV–vis spectrophotometer (TU-1901) at a maximum absorption wavelength of 664 nm [39].

2.4 Characterizations

X-ray diffraction (XRD) data for Bi₂MoO₆, Ag/AgBr, and different proportions of Ag/AgBr–Bi₂MoO₆ were acquired using a Rigaku DMAX⁻ Ultima⁺ diffractometer at room temperature with CuK_α radiation (λ = 0.15406 nm). UV–vis diffuse reflectance spectroscopy (DRS) was measured using TU-1901 UV–vis spectrophotometer. Photoluminescence (PL) spectra were obtained on a Hitachi F-4600 fluorescence spectrophotometer with a 450 W Xe lamp as the excitation light source. The photoelectrochemical measurements were carried out in VMP3 electrochemical workstation. The electrolyte solution is Na₂SO₄ (0.1 M). SUPRA 55 SAPPHIRE field emission scanning electron microscopy and JEOL JEM-2100 transmission electron microscopy were used to examine the morphologies and crystal structures of the samples.

3 Results and Discussion

3.1 Characterization of As-Prepared Samples

Further information, such as crystal phase and crystallinity of samples with different contents of Ag/AgBr, has been determined by XRD analysis. As shown in Fig. 2, the strong diffraction angles at 2θ = 28.4°, 32.74°, 33.18°, 36.24°, 47.24°, 55.66°, 56.34°, and 58.6° can be assigned to (1 3 1), (2 0 0), (2 1 0), (1 5 1), (2 6 0), (3 3 1), (1 9 1), and (2 6 2) crystal planes of pure Bi₂MoO₆ by JCPDS (No. 84-0787) respectively. This condition showed that the Bi₂MoO₆ samples possess orthorhombic structure (a = 5.489 nm, b = 16.22 nm, and c = 5.513 nm). After modification by Ag/AgBr nanoparticles, several new diffraction peaks at 31.12°, 55.27°, and 73.58° were observed in the picture, which are assigned to the (2 0 0),

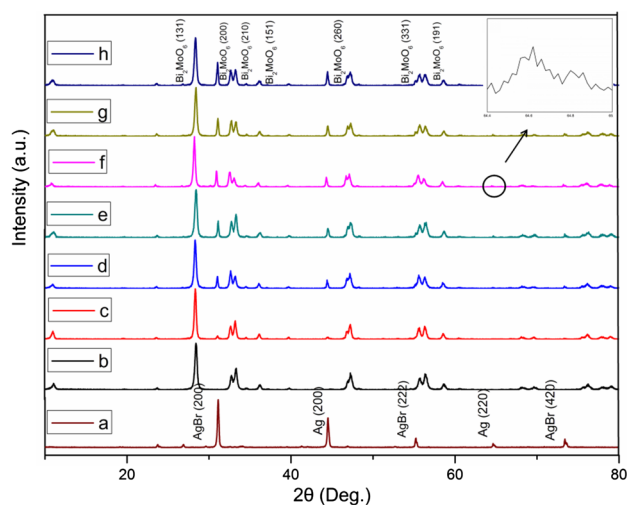


Fig. 2 The XRD patterns of *a* Ag/AgBr, *b* BMO, *c* BMO-10, *d* BMO-15, *e* BMO-20, *f* BMO-25, *g* BMO-30 and *h* BMO-35

(2 2 2), and (4 2 0) planes of AgBr crystal (No. 06-438), and the new peaks at 44.34° and 64.6° corresponding to (200) and (220) facets of Ag (No. 04-0783), respectively. The characteristic peaks have been strengthened with the increase of Ag/AgBr content, which indicates that the degree of Ag/AgBr crystallization improved accordingly. In addition, no other peaks have been detected, indicating the high purity of the chemical composition.

X-ray photoelectron spectroscopy (XPS) was used to determine the elemental composition of as-prepared sample (Fig. 3a), revealing strong peaks of Bi 4f, Mo 3d, Ag 3d, O 1s and Br 3d. Figure 3b shows the binding energy values of Bi 4f_{7/2} and Bi 4f_{5/2} are observed at 159.2 and 164.5 eV. Two peaks at 232.4 and 235.4 eV are observed in Fig. 3d, which are assigned to Mo 3d_{5/2} and Mo 3d_{3/2}, respectively. Figure 3d gives the peaks located at 367.6 and 373.7 eV are for Ag 3d_{5/2} and Ag 3d_{3/2}. Each of peaks were further deconvoluted into 367.6/368.1 and 373.7/374.2 eV two peaks, which can be attributed to Ag⁺ and Ag⁰, respectively. Figure 3e reveals that the peaks at 68.7 and 69.7 eV can be ascribed to Br 3d_{5/2} and Br 3d_{3/2} [40]. The XPS results verify the existence of Ag⁰.

Figure 4 represents the SEM and HRTEM images of Bi₂MoO₆ and Ag/AgBr–Bi₂MoO₆ composites. As indicated in Fig. 4a, the irregular layer structure of Bi₂MoO₆ with a side length of 60–300 nm has been revealed. The surface smooth plate-like structure can be obtained easily. The morphology of precursor does not change after decorating by Ag/AgBr as shown in Fig. 4b. This condition indicated that the introduction of Ag/AgBr did not change the orientation of growth of Bi₂MoO₆. Moreover, the nanoparticles with small size attached to the surface of

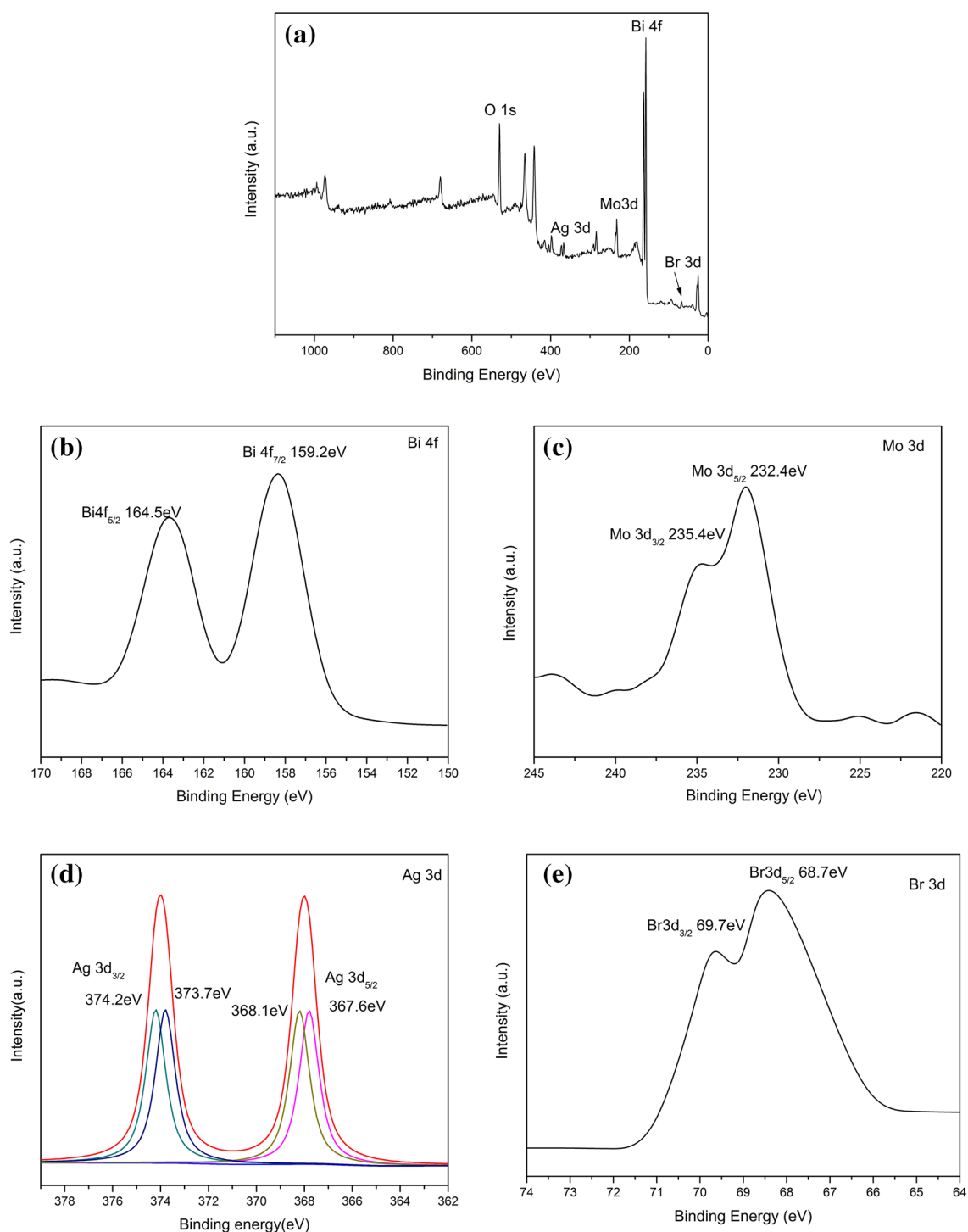


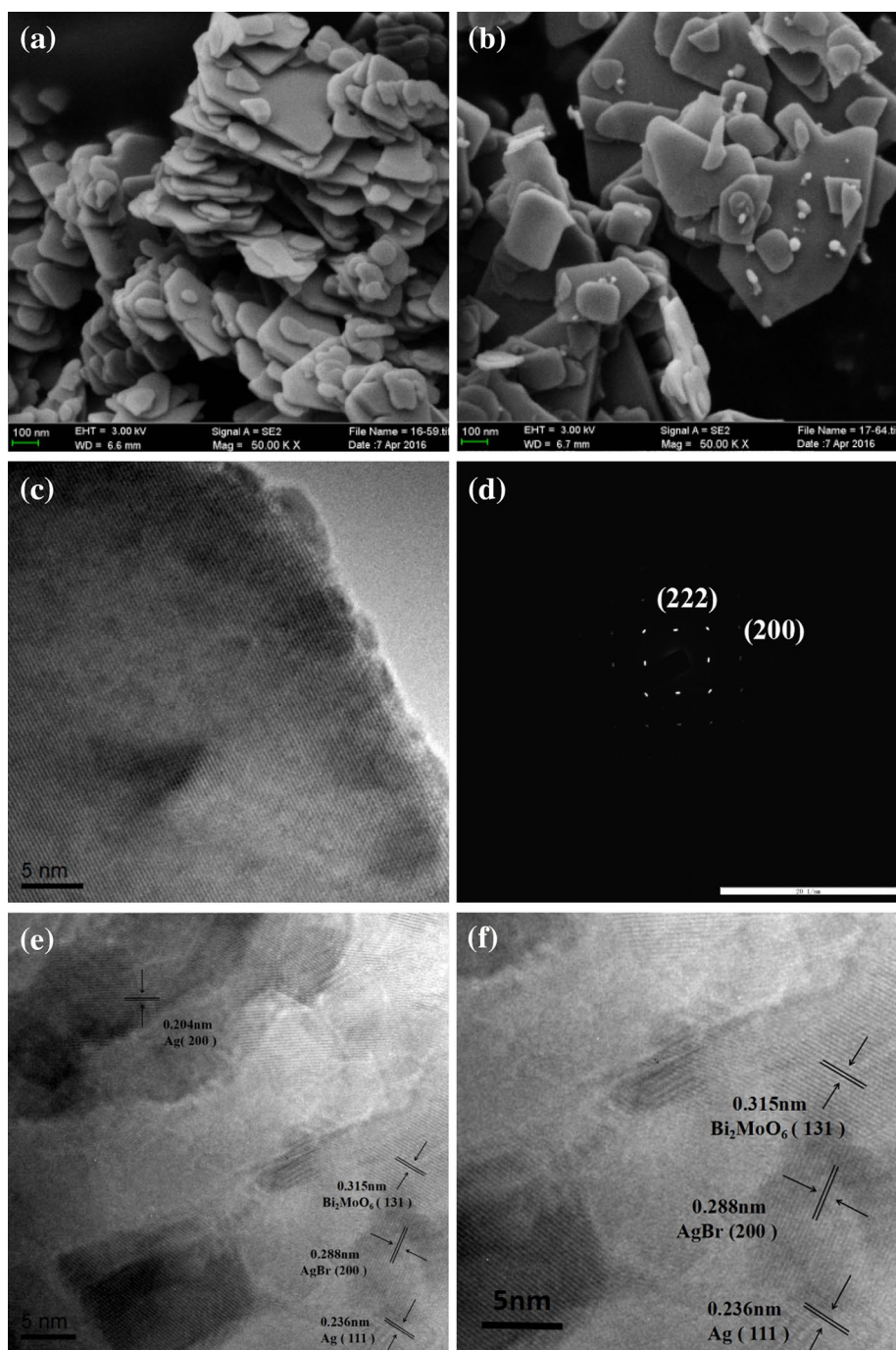
Fig. 3 X-ray photoelectron survey (a), high resolution XPS spectra of **b** Bi 4f, **c** Mo 3d, **d** Ag 3d, **e** Br 3d. (Color figure online)

Bi_2MoO_6 were detected in Fig. 4b, demonstrating the successful doping of Ag/AgBr.

The distinct fringes spaced by ~ 0.315 nm corresponded to the (131) planes of Bi_2MoO_6 , as shown in Fig. 4c. Figure 4d shows the regular square diffraction spot array

of individual Bi_2MoO_6 , which is the evidence of single-crystalline species. In the present analysis, SEAD was indexed to the (200) and (222) planes projected along the [100] zone axis. The morphology and structure information of BMO-25 are shown in Fig. 4e, f. The lattice fringe

Fig. 4 SEM images of **a** BMO, **b** BMO-25 and HRTEM images of **c** BMO, **d** SEAD pattern of BMO, **e, f** HRTEM images of BMO-25



spacing of about 0.288 nm was indexed for (200) facet of AgBr, and those of 0.204 and 0.236 nm were identified as the existence of (200) and (111) planes of Ag, respectively. In accordance with the experiment results, Ag/AgBr– Bi_2MoO_6 microstructure was formed after the interaction between Ag/AgBr and Bi_2MoO_6 at the place of two samples' contact surface. This condition is beneficial to improve the photocatalytic activity of the composite. The reason will be analyzed on the basis of experimental data later.

The UV–vis DRS used as a method to study the optical response of sample, and plots for $(\alpha h\nu)^2$ versus energy ($h\nu$) of BMO and BMO-25 are shown in Fig. 5. The absorption of Bi_2MoO_6 is 470 nm, indicating that Bi_2MoO_6 can be used as visible light photocatalyst. After decorating by Ag/AgBr, the absorption of sample enhanced in both the visible and ultraviolet regions with a slight absorption red-shift. The band gap energy of prepared catalysts can be calculated by the formula:

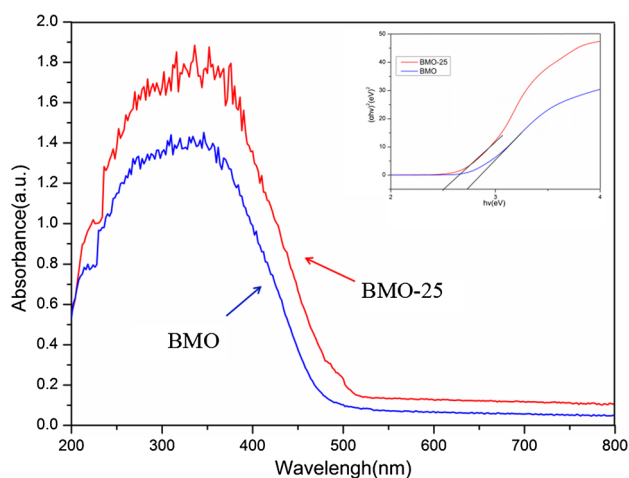


Fig. 5 UV-vis DRS spectra of BMO and BMO-25. (Color figure online)

$$\alpha(h\nu)^2 = A(h\nu - E_g)^{1/2}$$

where α is the absorption coefficient, and E_g is energy band gap of the semiconductor. In accordance with the equation, plots of $(\alpha h\nu)^2$ versus energy ($h\nu$) of BMO and BMO-25 are shown in Fig. 5. From the tangent line of the curve, E_g of BMO and BMO-25 was 2.65 and 2.51 eV, respectively. And the conclusion was that the introduction of Ag/AgBr species enhanced the absorption ability to visible light, which exhibits great influence on photocatalytic performance. The mechanism of improvement is related to the SPR effect of Ag [41, 42] and the interaction between Ag/AgBr and Bi_2MoO_6 .

3.2 Photocatalytic Activity

The photocatalytic activities of the novel samples are investigated by the photodegradation of organic dyes with visible light. MB was selected as target to demonstrate the degradation ability of the photocatalysts in this study. The procedure of sampling the pollutant solution MB was processed under the same identical conditions. Moreover, the samples were used to record the impact of all the composites that act on MB by UV-vis absorption spectrum. Figure 6a shows that the performance of Ag/AgBr- Bi_2MoO_6 in MB degradation increases with the percentage of Ag/AgBr increasing, whereas the phenomenon moved in the opposite direction when the Ag/AgBr content is higher than 25 wt%. Thus, the 25 wt% Ag/AgBr- Bi_2MoO_6 has been chosen as the specimen for further study because of its best performance. In addition, the degradation rate constant of MB was presented in histogram, which assures that the science data is indicative. The apparent rate constant k of Ag/AgBr, Bi_2MoO_6 , BMO-10, BMO-15, BMO-20, BMO-25, BMO-30, and BMO-35 is 0.4959, 0.1109, 0.1589, 0.4338, 0.6088, 0.8698, 0.371, and 0.2744 h^{-1} , respectively. The degradation rate constant of 25 wt% Ag/AgBr- Bi_2MoO_6 was 7.8 times higher than that of pure Bi_2MoO_6 , which proves that the interaction between the Ag/AgBr and Bi_2MoO_6 is the key factor to improve the catalytic activity.

The photoelectrocatalytic degradation at 2 V bias potential for BMO-25 and BMO samples are shown in Fig. 6b. The activities of all samples improved significantly by using external bias voltage compared with photocatalytic activities. The degradation ratio of BMO-25 can reach up to 97% within 60 min at the same experimental environment. Comparing the data of BMO and BMO-25 under the

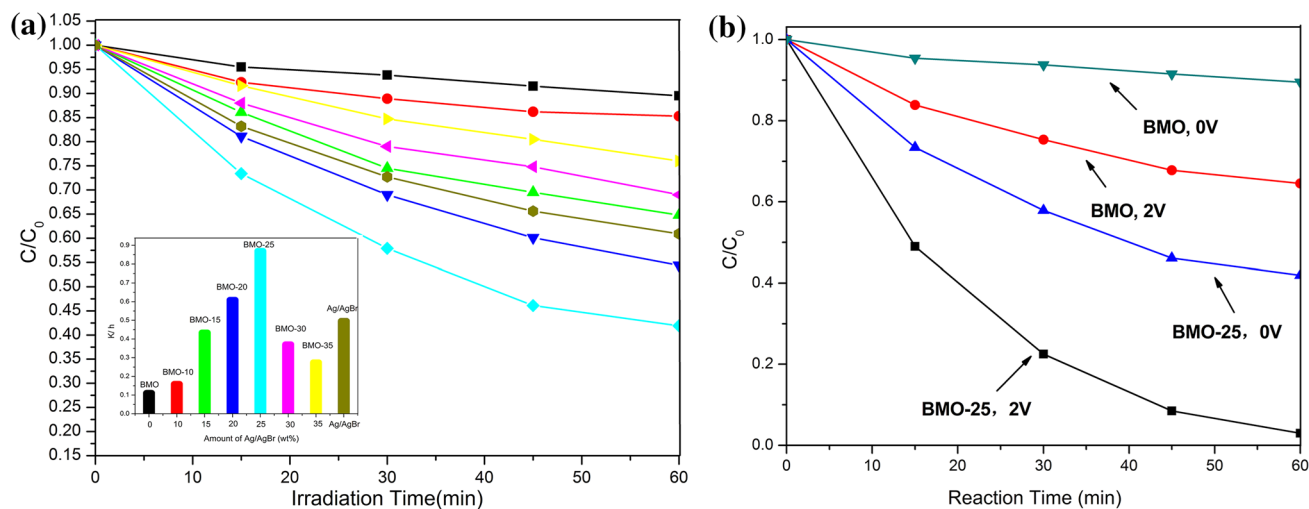


Fig. 6 **a** Photocatalytic decolorization of MB with different samples under visible-light irradiation and the degradation rate constant, **b** photoelectrocatalytic degradation of MB for BMO-25 and BMO samples under 2 V bias potential or not. (Color figure online)

condition of 2 V bias voltage, the conclusion that the introduction of Ag/AgBr species is also beneficial to the photoelectrocatalytic property of Bi_2MoO_6 was got easily. The mechanism of improvement will be discussed later.

The reusable performance of catalyst is always considered when the products were used for practical applications [43]. The experiments were recycled five times to test the stability of BMO-25 films at the same experimentation. As shown in Fig. 7, the degradation rate changed slightly between the recycle and contrast experiments, which was attributed to the stability of as-prepared samples. This feature enables the long reusable life of the BMO-25 composite.

3.3 Photocatalytic Mechanism Discussion

Several factors can influence the catalytic activity of semiconductors distinctly, such as surface area (adsorption activity), crystal phase, intensity, and electronic properties (separation efficiency of the electrons and holes, and so on). Electrochemical impedance spectroscopy (EIS) experiments have been applied to indicate the separation efficiency of the electrons and holes driven by sunlight in composite photocatalysts [44]. The results of EIS experiments on BMO/BMO-25 electrodes with and without visible light irradiation ($\lambda > 420$ nm) are shown in Fig. 8. The conclusion is that the electron–hole pairs irradiated by visible light of BMO-25 can separate and transfer to sample surface much easier compared with pure BMO. This condition results from the smaller diameter of the arc radius on Nyquist plots of the BMO-25 electrode than that of the BMO electrode. Further, this phenomenon is attributed to the interfacial interaction between Ag/AgBr and Bi_2MoO_6 ,

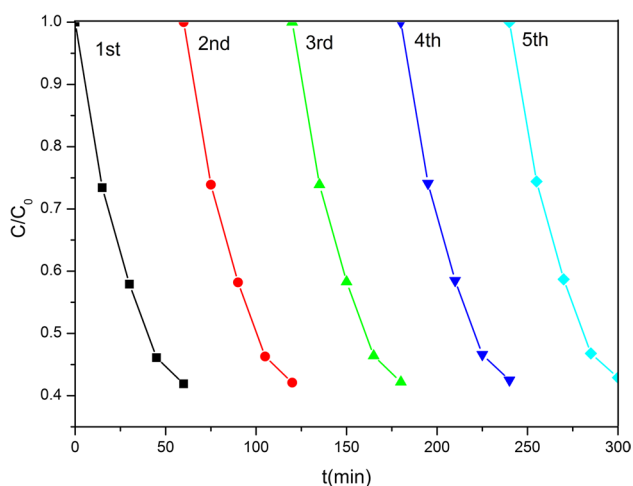


Fig. 7 Photocatalytic activity of the reused BMO-25 composites for five cycles. (Color figure online)

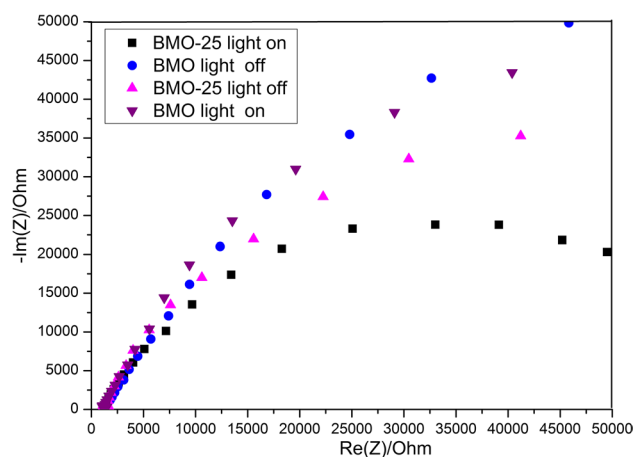


Fig. 8 Electrochemical impedance spectroscopy (EIS) Nyquist plots of BMO, BMO-25 and Ag/AgBr electrodes under the condition of light on/off ($\lambda > 420$ nm)

which is beneficial to separate efficiently the photoinduced electrons and holes.

Photoluminescence spectra also can be used to demonstrate the recombination processes of the pairs of electrons and holes. The PL emission spectrum (Fig. 9) measured at an excitation light of $\lambda = 395$ nm of BMO and BMO-25 indicates that the emission peaks of samples centered at around 460 nm. In addition, the PL emission intensity of BMO-25 is lower than that of BMO. The spectra made it practical to draw the conclusion that the recombination efficiency has been controlled effectively by introducing Ag/AgBr species, which corresponds to the conclusion of EIS experiments.

In accordance with the result of XRD, the diffraction peaks at $2\theta = 28.4^\circ$ and 32.74° (corresponding to (131) and

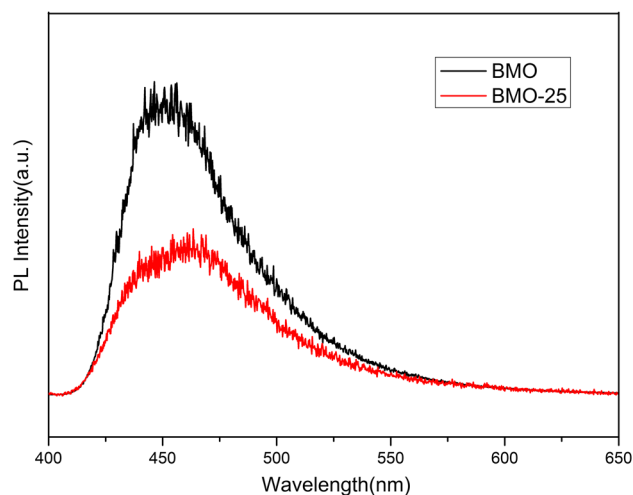


Fig. 9 Photoluminescence spectra (PL) of BMO and BMO-25. (Color figure online)

(200) crystal planes of pure Bi_2MoO_6 , respectively) are more intense than others, and the value of $I(131)/I(200)$ is less than two when the sample was synthesized in acid condition basically. This result reveals that the (200) plane with several composite structures has achieved optimum growth [45]. Thus, (200) plane was chosen as the target to elaborate the mechanism. Moreover, the H^+ in acid solution was absorbed on (200) plane because of the existence of several unsaturated oxygen, which develops Bi_2MoO_6 along the (200) plane. In addition, the Ag/AgX species could have attached to this plane when they were introduced, as shown in Fig. 10.

The exploration of possible migration routes of the photogenerated electron-holes pairs is beneficial for explaining the enhanced photocatalytic activity. The crystal thickness have been designed about 5 angstrom when build Ag/AgBr- Bi_2MoO_6 model. And the vacuum layer thickness has been designed 10 angstrom. Also, experimental and computational methods are the most common way to explore the mechanism. Conduction band (CB) and valence band (VB) potentials of Bi_2MoO_6 were calculated by the following equations [46]:

$$E_{\text{CB}} = X - E_e - 0.5 E_g \quad (1)$$

$$E_{\text{VB}} = E_{\text{CB}} + E_g \quad (2)$$

where X is the geometric mean of the Mulliken's electronegativities of the semiconductor; and E_e is the energy of free electrons on the hydrogen scale (~ 4.5 eV). The value of CB and VB potentials of Bi_2MoO_6 are -1.13 and 1.57 eV respectively, which are calculated by Eqs. (1) and (2); whereas those of AgBr are estimated to be -0.3 and 2.3 eV, respectively. Ag nanoparticles, whose absorption peak is at the range of visible light, can generate the pairs of electrons and holes after absorbing the energy of visible light with the effect of SPR when exposed to irradiation. Bi_2MoO_6 , a semiconductor with a narrow band gap, can be also irradiated in the range of visible light.

With further analysis, the explanation is based on the first principle calculation. All the calculations were performed by the CASTEP package. To calculate the electronic density of states, we used a plane wave cutoff energy of 340 eV and $5 \times 4 \times 5$ k -point for Bi_2MoO_6 , 340 eV, and $5 \times 2 \times 5$ k -point for Bi_2MoO_6 (200) plane and Ag (111) plane. The work function of Bi_2MoO_6 (200) plane and Ag (111) plane are 2.486 eV (named as W_s) and 3.331 eV (named as W_m) respectively, which was calculated based on first principle. Thus, electrons should transfer from semiconductor to the metal based on the theory that W_m is greater than W_s and $(E_f)_m$ is less than $(E_f)_s$. However, the real transfer routes of the photoexcited electrons flow inversely. The reason can be explained as follows: the e^- on Ag nanoparticle surface was in the excited states after irradiation by visible light, and obtained energy during this procedure with the effect of SPR. The energy of hot electrons waved around its own Fermi level and the range of the vibration was from 1.0 to 4.0 eV [47]. Hence, because of this special reaction, the excited electrons accumulated in Ag nanoparticles have enough energy for the migration that from Ag nanoparticles to CB of Bi_2MoO_6 and AgBr. Subsequently, the electrons (including those coming from Ag nanoparticles) in AgBr and Bi_2MoO_6 were trapped to form $\cdot\text{OH}$ and $\cdot\text{O}_2^-$ after reacting with O_2 and H_2O . $\cdot\text{OH}$ radical species have succeeded in converting MB directly into H_2O , CO_2 , and other inorganic molecules, just as you can seen in Fig. 11. In addition, the photodegradation process of organic dye can proceed smoothly, which can be described as follows:

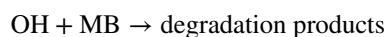
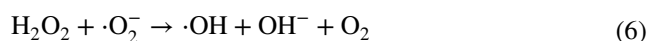


Fig. 10 Molecular structure of Ag/AgBr- Bi_2MoO_6

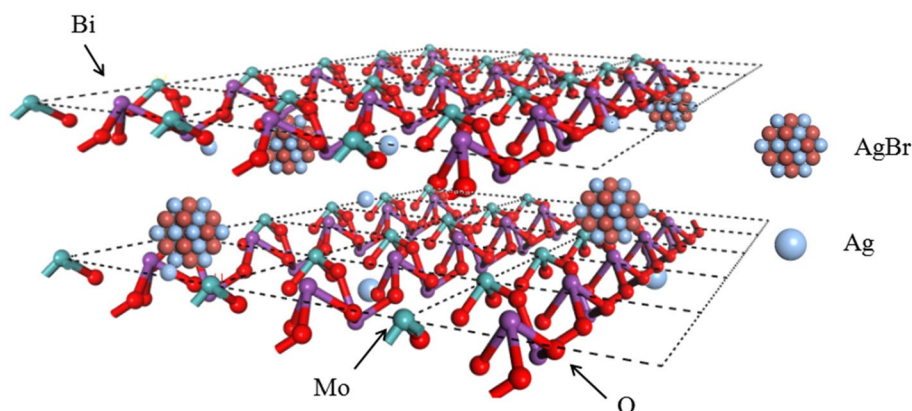
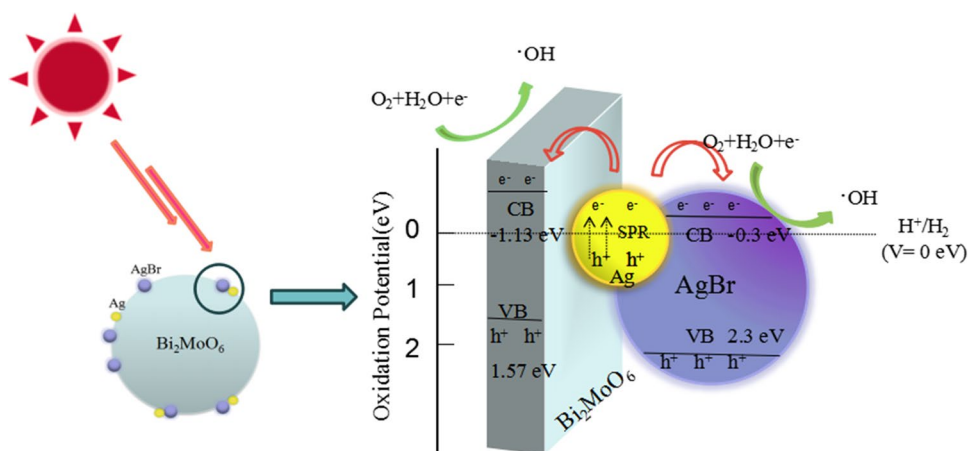


Fig. 11 Schematic diagram of the transfer of photogenerated electrons over Ag/AgBr–Bi₂MoO₆ samples with SPR effect



The result of property test is that the photocatalytic activities of all Ag/AgBr–Bi₂MoO₆ hybrids were better than that of pure Bi₂MoO₆. The performance of Ag/AgBr–Bi₂MoO₆ sample increased as more Ag/AgBr particles were mixed. When the content of Ag/AgBr was higher than 25 wt%, the result is opposite. The reason is that the anchored force between the Bi₂MoO₆ and Ag/AgBr weakens gradually with the increasing size of Ag/AgBr nanoparticle. Moreover, this character could destruct the heterojunction structure, which may play an important role in the photodegradation process [48]. Thus, 25% Ag/AgBr–Bi₂MoO₆ showed the best photocatalytic activity compared with other Ag/AgBr–Bi₂MoO₆ photocatalysts in this study.

The space-charge layer came into being at semiconductor/solution interface after immersing in the electrolyte solution. In addition, the Schottky barrier formed in the meantime. The newly formed Schottky barrier drives electrons and holes motivated by visible light transfer in the opposite direction, which achieved the efficient separation of electric charges and decreased the recombination of the photogenerated electrons and holes. Under the effect of external biasing voltage, electrons transfer from semiconductor carrier substrates to Ti electrode, and the electrons were trapped by O₂ and H₂O to form ·OH, as shown in Fig. 12. The next reaction in MB solution is similar to the reaction taking place in photocatalysis experiments. Moreover, lots of electrons come from Ag nanoparticles making the degradation process to continue easily. The introduction of Ag/AgBr species is beneficial to both photocatalytic and photoelectrocatalytic performance of Bi₂MoO₆.

4 Conclusions

Ag/AgBr–Bi₂MoO₆ composites were synthesized by depositing Ag/AgBr nanocrystals. Moreover, the high photocatalytic performance sample was made into films

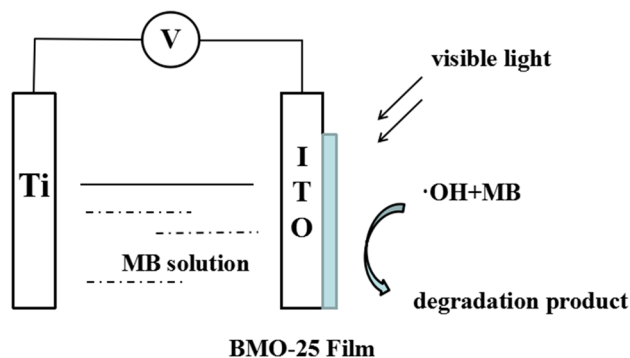


Fig. 12 Photoelectrocatalytic degradation mechanism of MB by Ag/AgBr–Bi₂MoO₆ film electrodes

for practical applications. Results showed that 25 wt% Ag/AgBr–Bi₂MoO₆ revealed the highest photocatalytic activity, whose degradation rate constant is 7.8 times higher than that of the pure Bi₂MoO₆. Thus, the Ag/AgBr nanoparticles attached to the surface of the Bi₂MoO₆ enable charge carriers to transfer rapidly and restrain the recombination of electron–hole pairs. In addition, the synergistic effect between Ag/AgBr and Bi₂MoO₆ was proven to be a vital factor to enhance the photocatalytic property of Ag/AgBr–Bi₂MoO₆. This work provides an efficient way to synthesize novel photocatalysts, which can be used in real applications in water pollution purification.

Acknowledgements This work is supported by the National Nature Science Foundation of China (No. 21276036), National Key Technology Support Program (2014BAB12B06), Program for Liaoning Excellent Talents in University (No. LJQ2015013) and the Fundamental Research Funds for the Central Universities (Nos. 3132016065 and 3132016341).

References

- B. O'Regan, M. Gratzel, A low-cost high-efficiency solar cell based on dye-sensitized colloidal TiO₂ films. *Nature* **353**, 737–740 (1991)
- S. Chavadej, P. Phuapromyod, E. Gulari, P. Rangsunvigit, T. Sreethawong, Photocatalytic degradation of 2-propanol by using Pt/TiO₂ prepared by microemulsion technique. *Chem. Eng. J.* **137**, 489–495 (2008)
- Y.J. Liu, F. Zhou, S. Zhan, Y.F. Yang, Y.F. Yin, Significantly enhanced performance of g-C₃N₄/Bi₂MoO₆ films for photocatalytic degradation of pollutants under visible-light irradiation. *Chem. Res. Chin. Univ.* **32**, 287–290 (2016)
- Q.C. Liu, D.K. Ma, Y.Y. Hu, Y.W. Zeng, S.M. Huang, Various bismuth oxyiodide hierarchical architectures: alcoholthermal controlled synthesis, photocatalytic activities, and adsorption capabilities for phosphate in water. *Appl. Mater. Interfaces* **5**, 11927–11934 (2013)
- F. Zuo, K. Bozhilov, R.J. Dillon, L. Wang, P. Smith, X. Zhao, C. Bardeen, P. Feng, Active facets on titanium(III)-doped TiO₂: an effective strategy to improve the visible-light photocatalytic activity. *Angew. Chem. Int. Ed.* **51**, 6223–6226 (2012)
- J. Schneider, M. Matsuoka, M. Takeuchi, J. Zhang, Y. Horiuchi, M. Anpo, D.W. Bahnemann, Understanding TiO₂ photocatalysis: mechanisms and materials. *Chem. Rev.* **114**, 9919–9986 (2014)
- J.J. Fan, L. Zhao, J.G. Yu, G. Liu, The effect of calcination temperature on the microstructure and photocatalytic activity of TiO₂-based composite nanotubes prepared by an in situ template dissolution method. *Nanoscale* **4**, 6597–6603 (2012)
- Y. Wang, J.G. Yu, W. Xiao, Q. Li, Microwave-assisted hydrothermal synthesis of graphene based Au–TiO₂ photocatalysts for efficient visible-light hydrogen production. *J. Mater. Chem. A* **2**, 3847–3855 (2014)
- L. Ge, C.C. Han, J. Liu, Novel visible light-induced g-C₃N₄/Bi₂WO₆ composite photocatalysts for efficient degradation of methyl orange. *Appl. Catal. B* **108**, 100–107 (2011)
- J.L. Lv, K. Dai, J.F. Zhang, L. Geng, C.H. Liang, Q.C. Liu, G.P. Zhu, C. Chen, Facile synthesis of Z-scheme graphitic-C₃N₄/Bi₂MoO₆ nanocomposite for enhanced visible photocatalytic properties. *Appl. Surf. Sci.* **358**, 377–384 (2015)
- J. Tian, P. Hao, N. Wei, H.Z. Cui, H. Liu, 3D Bi₂MoO₆ nanosheet/TiO₂ nanobelt heterostructure: enhanced photocatalytic activities and photoelectrochemistry performance. *ACS Catal.* **5**, 4530–4536 (2015)
- Y. Shimodaira, H. Kato, H. Kobayashi, A. Kudo, Photo-physical properties and photocatalytic activities of bismuth molybdates under visible light irradiation. *J. Phys. Chem. B* **110**:17790–17797 (2006)
- C.S. Guo, J. Xu, S.F. Wang, L. Li, Y. Zhang, X.C. Li, Facile synthesis and photocatalytic application of hierarchical mesoporous Bi₂MoO₆ nanosheet-based microspheres. *Cryst. EngComm* **14**, 3602–3608 (2012)
- M. Shang, W. Wang, J. Ren, S. Sun, L. Zhang, Nanoscale Kirkendall effect for the synthesis of Bi₂MoO₆ boxes via a facile solution-phase method. *Nanoscale* **3**(4), 1474–1476 (2011)
- C. Kongmark, R. Coulter, S. Cristol, A. Rubbens, C. Pirovano, A. Lofberg, G. Sankar, W.V. Beek, E.B. Richard, R.N. Vannier, A comprehensive scenario of the crystal growth of γ -Bi₂MoO₆ catalyst during hydrothermal synthesis. *Cryst. Growth Des.* **12**, 5994–6003 (2012)
- J.L. Lv, J.F. Zhang, L. Geng, C.H. Liang, Q.C. Liu, G.P. Zhu, C. Chen, Facile synthesis of Z-scheme graphitic-C₃N₄/Bi₂MoO₆ nanocomposite for enhanced visible photocatalytic properties. *Appl. Surf. Sci.* **358**, 377–384 (2015)
- J.L. Li, X.J. Liu, Z. Sun, L.K. Pan, Novel Bi₂MoO₆/TiO₂ heterostructure microspheres for degradation of benzene series compound under visible light irradiation. *J. Colloid. Interface Sci.* **463**, 145–153 (2016)
- T.T. Zheng, J.Y. Xu, Z.J. Zhang, H.B. Zeng, P₃HT/Bi₂MoO₆ heterojunction with enhanced photocatalytic activity. *Mater. Lett.* **164**, 640–643 (2016)
- J. Zhao, Q.F. Lu, M.Z. Wei, C.Q. Wang, Synthesis of one-dimensional α -Fe₂O₃/Bi₂MoO₆ heterostructures by electrospinning process with enhanced photocatalytic activity. *J. Alloys Compd.* **15**, 417–424 (2015)
- C.L. Yu, Z. Wu, R.Y. Liu, H.B. He, W.H. Fan, S.S. Xue, The effects of Gd³⁺ doping on the physical structure and photocatalytic performance of Bi₂MoO₆ nanoplate crystals. *J. Phys. Chem. Solids* **93**, 7–13 (2016)
- A.A. Alemi, R. Kashfi, B. Shabani, Preparation and characterization of novel Ln (Gd³⁺, Ho³⁺ and Yb³⁺)-doped Bi₂MoO₆ with Aurivillius layered structures and photocatalytic activities under visible light irradiation. *J. Mol. Catal. A* **392**, 290–298 (2014)
- L.R. Hou, H. Hua, L.K. Gan, G.Z. Yuan, Template-free solvothermal fabrication of hollow Bi₂MoO₆ microspheres with enhanced visible light photocatalytic activity. *Mater. Lett.* **159**, 35–38 (2015)
- L.W. Zhang, T.G. Xu, X. Zhao, Y.F. Zhu, Controllable synthesis of Bi₂MoO₆ and effect of morphology and variation in local structure on photocatalytic activities. *Appl. Catal. B* **98**, 138–146 (2010)
- J.L. Li, X.J. Liu, Z. Sun, L.K. Pan, Mesoporous yolk-shell structure Bi₂MoO₆ microspheres with enhanced visible light photocatalytic activity. *Ceram. Int.* **41**, 8592–8595 (2015)
- X. Ding, W.K. Ho, J. Shang, L.Z. Zhang, Self doping promoted photocatalytic removal of no under visible light with Bi₂MoO₆: Indispensable role of superoxide ions. *Appl. Catal. B* **182**, 316–325 (2016)
- Z.J. Zhang, W.Z. Wang, D. Jiang, J.Y. Xu, CuPc sensitized Bi₂MoO₆ with remarkable photo-response and enhanced photocatalytic activity. *Catal. Commun.* **55**, 15–18 (2014)
- Y.G. Xu, H. Xu, H.M. Li, J.X. Xia, C.T. Liu, L. Liu, Enhanced photocatalytic activity of new photocatalyst Ag/AgCl/ZnO. *J. Alloys Compd.* **509**, 3286–3292 (2011)
- J.F. Guo, B.W. Ma, A.Y. Yin, K.N. Fan, W.L. Dai, Photodegradation of rhodamine B and 4-chlorophenol using plasmonic photocatalyst of Ag–AgI/Fe₃O₄@SiO₂ magnetic nanoparticle under visible light irradiation. *Appl. Catal. B* **101**, 580–586 (2011)
- M.S. Zhu, P.L. Chen, M.H. Liu, Ag/AgBr/graphene oxide nanocomposite synthesized via oil/water and water/oil microemulsions: a comparison of sunlight energized plasmonic photocatalytic activity. *Langmuir* **28**, 3385–3390 (2012)
- G.Q. Luo, X.J. Jiang, M.J. Li, Q. Shen, L.M. Zhang, H.G. Yu, Facile fabrication and enhanced photocatalytic performance of Ag/AgCl/rGO heterostructure. photocatalyst. *ACS Appl. Mater. Interfaces* **5**, 2161–2168 (2013)
- D.F. Xu, B. Cheng, J.F. Zhang, W.K. Wang, J.G. Yu, W.K. Ho, Photocatalytic activity of Ag₂MO₄ (M^{1/4} Cr, MoW) photocatalysts. *J. Mater. Chem. A* **3**, 20153–20166 (2015)
- H. Cheng, B. Huang, P. Wang, Z. Wang, Z. Lou, J. Wang, X. Qin, X. Zhang, Y. Dai, ion exchange synthesis of the novel Ag/AgBr/BIOBr hybrid with highly efficient decontamination of pollutants. *Chem. Commun.* **47**, 7054–7056 (2011)
- K. Fuku, R. Hayashi, S. Takakura, T. Kamegawa, K. Mori, H. Yamashita, The synthesis of size- and color-controlled silver nanoparticles by using microwave heating and their enhanced catalytic activity by localized surface plasmon resonance. *Angew. Chem. Int. Ed.* **52**, 7446–7450 (2013)

34. S. Linic, P. Christopher, D.B. Ingram, Plasmonic-metal nanostructures for efficient conversion of solar to chemical energy. *Nat. Mater.* **10**, 911–921 (2011)
35. S. Bai, J. Jiang, Q. Zhang, Y.J. Xiong, Steering charge kinetics in photocatalysis: intersection of materials syntheses, characterization techniques and theoretical simulations. *Chem. Soc. Rev.* **44**, 2893–2939 (2015)
36. J. Li, W. Fang, C. Yu, W. Zhou, L. Zhu, Y. Xie, Ag-based semiconductor photocatalysts in environmental purification. *Appl. Surf. Sci.* **358**, 46–56 (2015)
37. Q. Sun, X.R. Jia, X.F. Wang, H.G. Yu, J.G. Yu, Facile synthesis of porous Bi_2WO_6 nanosheets with high photocatalytic performance. *Dalton Trans.* **44**, 14532–14539 (2015)
38. K. Dai, D.P. Li, L.H. Lu, Q. Liu, C.H. Liang, J.L. Lv, G.P. Zhu, Plasmonic $\text{TiO}_2/\text{AgBr}/\text{Ag}$ ternary composite nanosphere with heterojunction structure for advanced visible light photocatalyst. *Appl. Surf. Sci.* **314**, 864–871 (2014)
39. F. Zhou, R. Shi, Y.F. Zhu, Significant enhancement of the visible photocatalytic degradation performance of Bi_2MoO_6 nanoplate by graphene hybridization. *J. Mol. Catal. A* **340**, 77–82 (2011)
40. J. Lv, K. Dai, J.Z. Zhang, L.H. Lu, C.H. Liang, L. Geng, Z.L. Wang, G.Y. Yuan, G.P. Zhu, In situ controllable synthesis of novel surface plasmon resonance-enhanced $\text{Ag}_2\text{WO}_4/\text{Ag}/\text{Bi}_2\text{MoO}_6$ composite for enhanced and stable visible light photocatalyst. *Appl. Surf. Sci.* **391**, 507–515 (2016)
41. P. Wang, B.B. Huang, X.Y. Qin, X.Y. Zhang, Y. Dai, J.Y. Wei, M.H. Whangbo, Ag@AgCl : a highly efficient and stable photocatalyst active under visible light. *Angew. Chem.* **120**, 8049–8051 (2008)
42. J.G. Hou, C. Yang, Z. Wang, Q.H. Ji, Y.T. Li, G.C. Huang, S.Q. Jiao, H.M. Zhu, Three-dimensional Z-scheme $\text{AgCl}/\text{Ag}/\gamma\text{-TaON}$ heterostructural hollow spheres for enhanced visible-light photocatalytic performance. *Appl. Catal. B* **142**, 579–589 (2013)
43. R. Asahi, T. Morikawa, H. Irie, T. Ohwaki, Nitrogen-doped titanium dioxide as visible-light-sensitive photocatalyst: designs, developments and prospects. *Chem. Rev.* **114**, 9824–9852 (2014)
44. W.H. Leng, Z. Zhang, J.Q. Zhang, C.N. Cao, Investigation of the kinetics of a TiO_2 photoelectrocatalytic reaction involving charge transfer and recombination through surface states by electrochemical impedance spectroscopy. *J. Phys. Chem. B* **109**, 15008–15023 (2005)
45. M.Y. Zhang, C.L. Shao, J.B. Mu, et al. Hierarchical heterostructures of Bi_2MoO_6 on carbon nanofibers: controllable solvothermal fabrication and enhanced visible photocatalytic properties. *J. Mater. Chem.* **22**(2), 577–584 (2012)
46. X. Zhang, Z.H. Ai, F.L. Jia, L.Z. Zhang, Generalized one-pot synthesis, characterization, and photocatalytic activity of hierarchical BiOX ($X=\text{Cl}, \text{Br}, \text{I}$) nanoplate microspheres. *J. Phys. Chem. C* **112**, 747–753 (2008)
47. S. Linic, P. Christopher, D.B. Ingram, Plasmonic-metal nanostructures for efficient conversion of solar to chemical energy. *Nat. Mater.* **10**, 911–921 (2011)
48. X.X. Li, S.M. Fang, L. Ge, C.H. Han, P. Qiu, W.L. Liu, Synthesis of flower-like $\text{Ag}/\text{AgCl}-\text{Bi}_2\text{MoO}_6$ plasmonic photocatalysts with enhanced visible-light photocatalytic performance. *Appl. Catal. B* **176–177**, 62–69 (2015)